5-9-2015

Detection of Local Extinction and Re-ignition in Non-premixed Ethylene-air Flames Using Chemical Explosive Mode Analysis

Cong Li
University of Connecticut - Storrs, licongcq@gmail.com

Detection of Local Extinction and Re-ignition in Non-premixed Ethylene-air Flames Using Chemical Explosive Mode Analysis

Cong Li

B.S., Peking University, 2013

A Thesis

Submitted in Partial Fulfillment of the

Requirements for the Degree of

Master of Science

At the

University of Connecticut

2015

2015

APPROVAL PAGE

Masters of Science Thesis

Detection of Local Extinction and Re-ignition in Non-premixed Ethylene-air Flames Using Chemical Explosive Mode Analysis

Presented by

Cong Li, B.S.

Major Advisor_____
Tianfeng Lu

Associate Advisor_____
Xinyu Zhao

Associate Advisor_____
Michael W. Renfro

University of Connecticut

2015

ACKNOWLEDGEMENTS

I would like to thank my advisor Prof. Tianfeng Lu for giving me the opportunity to study in UCONN and conduct research on combustion, and for his advice and pivotal support that have made this thesis possible.

I want to thank Dr. Xinyu Zhao and Dr. Michael W. Renfro as my thesis committee members for their help in my professional growth. I'm especially grateful for Dr. Zhao's advices on the DNS data analysis. Thank my collaborators Dr. David O. Lignell at the Brigham Young University and Dr. Jacqueline H. Chen at Sandia National Laboratories for providing the DNS data and their help in this study.

I would like to thank my colleagues Yufeng Liu, Chao Xu, Yunchao Wu, Yang Gao, Ruiqin Shan, Dr. Xianming Wang, Dr. Pengfei Li and Mike Kuron. Without their help, this work would not have been possible.

Finally, I would like to thank my parents for their support and love.

Table of Contents

Abstract

Extinction of 1-D laminar non-premixed counterflow flames and a 3-D turbulent non-premixed ethylene jet flame into air coflow is studied with chemical explosive mode analysis (CEMA), which is an eigen-analysis shown to be effective in systematic detection of critical flame features in a variety of combustion systems, e.g. auto-ignition, ignition and extinction in perfectly stirred reactors, and location of premixed reaction fronts. In the present study, CEMA-based criteria are proposed to systematically detect local extinction and re-ignition in non-premixed flames. The method is first demonstrated with 1-D laminar counterflow flames showing that mixtures in the reaction zone start to show explosive behavior, characterized by a positive eigenvalue of the chemical Jacobian, when the flame approaches extinction as strain rate increases, while only nonexplosive mixtures are present in strongly burning flames at low strain rates. Thus the existence of explosive mixtures provides a necessary condition to detect flame extinction. This criterion is further employed to study the direct numerical simulation (DNS) data from a 3-D non-premixed temporal turbulent ethylene-air jet flame. Local subdomains with strongly burning non-premixed flamelet, and near-extinction and post-extinction features are identified and investigated using CEMA-based diagnostics. Propagating premixed flame fronts are also identified in the re-ignition process of the globally non-premixed flame.

1. Introduction

Combustion energy accounts for more than 80 percent of the world's energy source [1], while it is also the major source of pollutant emissions such as carbon monoxide (CO), nitrogen oxides (NOx) and particulate matters. As such it is critical to design efficient and low-emission combustors, which subsequently requires a thorough understanding of the underlying chemical and physicochemical processes, including limit phenomena such as ignition and extinction, as well as other critical flame features such as premixed reaction fronts, non-premixed flame kernels and onset of flame instabilities. Local extinction and re-ignition may also occur at strongly turbulent flames at either premixed and non-premixed conditions and can have significant effects on global flame behaviors such as turbulent flame propagation and flame stabilization. For example, lean blowout as an extinction phenomenon has been a focal issue in industrial gas turbines and aero engines [2], which may occur at lean-burning conditions for improved fuel efficiency and/or reduced emissions.

Local extinction and re-ignition may frequently occur in non-premixed flames at increased strain rates, and a variety of methods have been developed in previous studies to detect local extinction in non-premixed flames. A theory for non-premixed flame extinction was first established by Liñán [3], extended in Refs. [4, 5], and reviewed in [6] to identify extinction in different flames. According to these studies, flame extinction is mainly characterized by a Damköhler number, defined as the ratio of a characteristic mixing timescale to a chemical timescale. In the flamelet modeling studies, extinction is determined by comparing the local scalar dissipation rate (SDR) with the extinction SDR of 1-D steady flames [7]. The model was extended to include parameters other than SDR to account for flame re-ignition in Ref. [8].

Integral effects of flow fluctuations on extinction was considered in Ref. [9]. A bifurcation analysis was recently developed based on eigen-analysis to rigorously define the extinction and ignition of steady state flames, and was demonstrated using perfectly stirred reactors (PSR) [10, 11].

In addition to these endeavors, experiments and computational fluid dynamics (CFD) also play critical roles in the understanding of flame extinction and re-ignition. In particular, high-fidelity numerical simulations can provide detailed flow information that is difficult to access in experiments. Typical methods for turbulent flame simulations include direct numerical simulation (DNS), large eddy simulations (LES) and Reynolds-averaged Navier-Stokes equations (RANS). DNS is based on the first principles and can provide complete information on reacting flows that is required for the diagnostics of many critical flame features. DNS has been employed to study the flame structures and stabilization mechanisms of different turbulent flames, using both one-step [12, 13] and detailed chemistry [14-16]. DNS data involving detailed chemistry can be extremely large and difficult to analyze. For instance, a 3-D DNS of a laboratory-scale lifted ethylene jet flame generated more than 240 terabytes of field and particle data [16]. Such a large dataset defies most flame diagnostic methods that require frequent human interactions. Systematic and robust methods are therefore needed to extract salient information from the massive DNS datasets.

Recently, a method of chemical explosive mode analysis (CEMA) [17] was developed to systematically detect critical flame features, including local ignition, extinction, and premixed flame fronts, in 0-D reactors, 1-D premixed flames and partially premixed turbulent lifted flames [17, 18], and homogeneous charge compression ignition (HCCI) combustion [19-22]. It was

found that CEMA-based criteria are robust and reliable for limit phenomena detection for premixed and partially premixed flames. Local extinction of a non-premixed turbulent DNS flame was also studied using a CEMA-based criterion and compared to that based on the activation energy asymptotic (AEA) theory by Lecoustre et al. [23]. Nevertheless, the behaviors of chemical explosive mode (CEM) in non-premixed flames remain not well-understood.

In the present study, non-premixed flame extinction and re-ignition will be systematically investigated using 1-D non-premixed counterflow flames to understand the behavior of the CEM in non-premixed flames. CEMA will then be utilized to diagnose the 3-D DNS dataset of a temporally evolving, non-premixed ethylene jet flame involving significant local extinction and re-ignition [15].

2. Review of the CEMA method

2.1 Formulation of CEMA

CEMA is based on eigen-analysis of the Jacobian of the chemical source term [17] of a spatially discretized reacting flow, for which the governing equation can be expressed as

$$\frac{d\boldsymbol{y}}{dt} = \boldsymbol{g}(\boldsymbol{y}) = \boldsymbol{\omega}(\boldsymbol{y}) + \boldsymbol{s}(\boldsymbol{y}) \tag{1}$$

where $\boldsymbol{y}$ is the vector of dependent variables, including temperature and species concentrations. $\boldsymbol{\omega}$ is the chemical source term, and $\boldsymbol{s}$ is the non-chemical source term, such as homogeneous mixing in perfectly stirred reactors (PSR), or the transport term in flames. The Jacobian of the right hand side of equation (1) thus consists of the contributions from the chemical and non-chemical source terms, respectively:

$$\boldsymbol{J_g} = \frac{\boldsymbol{\partial g(y)}}{\boldsymbol{\partial y}} = \boldsymbol{J_\omega} + \boldsymbol{J_s}, \;\; \boldsymbol{J_\omega} = \frac{\boldsymbol{\partial \omega(y)}}{\boldsymbol{\partial y}}, \;\; \boldsymbol{J_s} = \frac{\boldsymbol{\partial s(y)}}{\boldsymbol{\partial y}} \tag{2}$$

The chemical Jacobian, $\boldsymbol{J_\omega} = \partial\boldsymbol{\omega}/\partial\boldsymbol{y}$, consists of information on the chemical properties of the local reacting mixture, and has been a major information source for mechanism reduction with intrinsic low dimensional manifold (ILDM) [24], computational singular perturbation (CSP) [25] and quasi steady state approximation (QSSA) [26]. The chemical Jacobian is block-diagonal for multi-grid systems, because the chemical source term is only determined by local species concentrations and thermal properties. Therefore, eigen-analyses of the chemical Jacobian on different grids can be decoupled and performed grid-wise. The size of chemical Jacobian at each grid point is (K+1) by (K+1), where K is the number of species.

CEMA focuses on eigenvalues in the chemical Jacobian with positive real parts. Assuming that heat capacity is a constant, there are M+1 conservative modes (M is the number of participating elements), and thus M+1 zero eigenvalues in the chemical Jacobian, one being associated with energy conservation and the others with element conservation. CEMA excludes these conservative eigenvalues and sorts the real parts of the other eigenvalues in descending order. λ_e is defined as the real part of the first eigenvalue in the sorted list. A positive λ_e indicates that the mixture is explosive in nature and tends to ignite if isolated, and the associated chemical mode is named a chemical explosive mode (CEM). If no positive eigenvalue is present, the mixture is nonexplosive in nature and evolves toward chemical equilibrium. Pre-ignition fuel-air mixtures are typically explosive, while post-ignition mixtures are typically nonexplosive as shown in previous studies [17-19]. There, the zero-crossing of the first eigenvalue was employed to detect ignition points in auto-ignition, extinction and ignition in steady-state PSR, and reaction zone locations in premixed flames. The imaginary part of the first eigenvalue indicates the oscillation frequency and is not further investigated in the present study.

2.2 CEMA for auto-ignition, premixed flames and PSRs

CEMA has been employed to detect auto-ignition, premixed flame fronts, and extinction and ignition in steady-state perfectly stirred reactors (PSR) [17-19]. In present study, the previous applications of CEMA will be demonstrated with a 19-species reduced mechanism [27], which was further employed in the DNS of a lifted ethylene jet flame [15] that will be investigated later in Section 4.

Figure 1 shows the evolution of temperature and λ_e for the constant-pressure auto-ignition of ethylene-air mixtures. The color at each data point shows the magnitude of λ_e. The coloring scheme conforms to that in previous studies [17-19]. It can be observed that the pre-ignition mixtures are all explosive, carrying positive CEM eigenvalues (red circles). The CEM eigenvalue λ_e reaches its maximum during the rapid temperature increase and becomes negative after the ignition point when the mixture starts to approach the equilibrium. It is seen that the zero-crossing point of λ_e is almost identical to the inflection point of the temperature profile during ignition. Therefore, the zero-crossing point of λ_e can be used as a definition of ignition point for auto-ignition [17].

Figure 2 demonstrates the temperature profile of a 1-D planar freely propagating premixed flame of ethylene-air. The color of each data point shows the value of λ_e. In the preheat zone, the CEM eigenvalue increases as the mixtures are preheated approaching the reaction zone. λ_e becomes negative in the post-flame zone after the ignition. The temperature profile near the zero-crossing of λ_e shows a large curvature, indicating a large heat release rate which is the characteristic of the reaction zone. This observation has been employed to identify the locations of premixed reaction fronts in previous works [17-19].

PSRs are typical applications involving both ignition and extinction. The solution of a PSR is characterized by the "S"-curve as shown in Fig. 3. The flames on the upper branch and lower branch of the curve are physically stable, and the flames on the middle branch are unstable. The upper turning point on the "S"-curve is widely regarded as the extinction state and the lower turning point the ignition state. The color of the data points in Fig. 3a shows the magnitude of CEM eigenvalue. It is seen that on the upper branch, strongly burning and near-

equilibrium mixtures with large residence time are nonexplosive, while the mixtures become explosive when approaching the extinction turning point as the residence time decreases. The mixing term $\boldsymbol{s}(\boldsymbol{y})$ in Eq. (1) for PSR can be approximated as a diagonal matrix [19]:

$$\boldsymbol{J}_s = \frac{\partial \boldsymbol{s}(\boldsymbol{y})}{\partial \boldsymbol{y}} \approx -\frac{\mathbf{1}}{\boldsymbol{\tau}}\boldsymbol{I} \tag{3}$$

where $\boldsymbol{I}$ is the identity matrix and τ is the residence time. The corresponding eigenvalue of the full Jacobian can then be approximated as $\lambda_g = \lambda_e - 1/\tau$. The turning point can therefore be attributed to the timescale balancing between CEM and the homogeneous mixing process, i.e. $\lambda_e \approx 1/\tau$, which results in a singular full Jacobian. Therefore, the zero-crossing of $\lambda_g = \lambda_e - 1/\tau$ can be employed to determine the extinction state of PSRs. Figure 3b shows the magnitude of λ_g, and it can be observed that the zero-crossings of λ_g are nearly identical to the turning points of the "S"-curve.

While CEMA has been extensively studied for auto-ignition, PSR and premixed flame front detection, the behavior of CEM during non-premixed flame extinction is not well-understood. In the following sections, CEMA will be utilized to study the extinction of 1-D non-premixed counterflow flames, as well as DNS data of a temporally evolving turbulent ethylene jet flame involving local extinction and re-ignition.

3. CEMA for 1-D non-premixed counterflow flames

An "*S*"-curve for 1-D steady-state non-premixed counterflow flames at atmospheric pressure is first calculated and shown in Fig. 4a. The counterflow flames consist of a fuel stream of nitrogen-diluted ethylene (47.64% ethylene in mole) opposed to an oxidizer stream of nitrogen-diluted oxygen (30.53% oxygen in mole). Both inlets are at a temperature of 550K. The fuel and oxidizer properties are chosen to match the DNS flame that will be studied in Section 4. Figure 4a shows the temperature at the stoichiometric surface of each flame as a function of the global strain rate, defined as [28]:

$$a = \frac{2|V_O|}{L}\left(1 + \frac{|V_F|\sqrt{\rho_F}}{|V_O|\sqrt{\rho_O}}\right) \tag{4}$$

where V is the flow velocity, ρ is density, and L is the burner separation distance. Subscripts O and F indicate the oxidizer and fuel boundary, respectively.

The color of each data point in Fig. 4a indicates the local eigenvalue, λ_e, of the CEM on the stoichiometric surface. For simplicity, the value of λ_e for a nonexplosive mixture is set to be the least-negative eigenvalue associated with the non-conservative modes. It is seen that CEM is not present in strongly burning flames that are weakly strained, while it starts to appear when the solution approaches and crosses the extinction turning point, as indicated by the red colors. Note that similar observation was made in steady-state PSRs on the response of CEMs to the decreasing residence time [18, 19]. Figure 4b shows the stoichiometric point λ_e as a function of temperature. It shows that λ_e becomes positive as the flame approaches extinction and there is a

deviation of the zero-crossing of λ_e from the turning point. It can also be observed that beyond the extinction point, λ_e drops rapidly as the flame temperature decreases. The mixture remains explosive for a post-extinction flame, while the magnitude of the eigenvalue becomes smaller as temperature decreases.

Note that similar deviations between the zero-crossing of CEM eigenvalue and the turning points were also observed in PSRs. It is expected that the turning points of the counterflow flames can be accurately captured by including an appropriate local mixing timescale in the criterion, as discussed for PSR in the previous section. In previous studies of turbulent lifted flames using CEMA [17, 18], scalar dissipation rate (SDR), denoted as χ, has been employed as a characteristic mixing time to define a Damköhler number, $Da = \lambda_e/\chi$, to mimic the criterion for flame extinction in PSR. The use of SDR to measure local mixing timescale is however rather involved as found in a recent study of transient flame behaviors [29]. As such, we shall focus on the behavior of the CEM in non-premixed flame extinction in the present study, and leave the formulation of a more accurate local mixing time to future work.

Figure 4c shows the temperature profiles colored by the eigenvalue of CEM for four selected flames on the "S"-curve in Fig. 4a. Specifically, P1 is a strongly burning flame at a low strain rate, P2 is a near-extinction flame where CEM starts to emerge, P3 is the extinction state, and P4 and P5 are physically unstable flames in the middle branch that may not be relevant to practical extinction and re-ignition processes. It is seen that, in the strongly burning flame P1, the mixtures on the entire spatial profile are nonexplosive, as indicated by the blue colors. This is because, for strongly burning flames, the local mixing is sufficiently slow compared with chemistry, such that the mixtures at different locations remain near-equilibrium. The quasi-

steady non-premixed flamelet approach is thereby applicable for such strongly burning flames. As strain rate increases, e.g. at flame P2, the residence time of a fluid element in the reaction zone is significantly reduced, resulting in incomplete chemical reactions and increased reactant concentrations, and CEM consequently emerges as can be seen on the spatial profile of flame P2.

At the extinction turning point, P3, the extent of incomplete reaction reaches a critical state such that further decrease in residence time quenches the flame. Explosive mixtures can be observed over a wide domain of the flame, including the reaction zone where temperature is high. Explosive mixtures can also be observed in flame P4 and P5 on the middle branch of the S-curve, spanning the entire reaction zone. Therefore, the presence of explosive mixtures is an indicator of near- and post-extinction in non-premixed flames, similar to that observed in extinction of PSR [18, 19]. On the other hand, nonexplosive mixtures are also present in near- and post-extinction flames as seen in Fig. 4c. Such nonexplosive mixtures are primarily observed outside the reaction zones in the near- and post-extinction flames. As such, the CEMA-based diagnostics in the present study will be primarily focused on the reaction zones near the stoichiometric surface, where chemistry is most important in determining the flame behavior. In the following sections, the presence of explosive mixtures will be employed to identify near- and post-extinction flame segments in a 3-D DNS of a non-premixed turbulent ethylene jet flame.

4. CEMA for the 3-D temporal non-premixed jet flame

In this section, CEMA will be employed to investigate local extinction and re-ignition in a 3-D DNS of a temporally-evolving non-premixed jet flame of ethylene [15]. The flame configuration of the DNS will first be briefly reviewed.

4.1 DNS configuration

A 3-D DNS of temporally-evolving non-premixed jet flame of ethylene was performed in Ref. [15]. The initial flame consists of a slab of nitrogen-diluted ethylene flowing in the domain center in the *x*-direction. The surrounding air flows in the opposite direction on either side of the fuel stream. Nonreflecting outflow boundary condition is applied in the spanwise (y) direction, and periodic boundary conditions are applied in the streamwise (x) and transverse (z) directions. The initial thickness of the fuel layer is $H = 0.96\,mm$. The dimensions of the computational domain are $12H\ (x) \times 15H\ (y) \times 8H(z)$. A uniform grid size of $17\ \mu m$ is used to discretize the domain in each direction. The mean velocity difference between the fuel and air is $\Delta U = 196\,m/s$. The jet timescale is defined as $\tau_{jet} = H/\Delta U = 0.0049\,ms$, and the jet Reynolds number is $Re_j = 5120$. Hyperbolic tangent profiles of velocity and mixture fraction are used to provide smooth transition of the velocity and mixture fraction differences between the fuel core and surrounding oxidizer flow. The transition thickness is $0.19\,mm$ for the velocity profile, and $0.74\,mm$ for the mixture fraction profile. The gas composition and temperature are determined through the mixture fraction profile. Isotropic turbulence is imposed on the initial velocity field in the fuel core. And the flames in the mixing layers are initialized with a 1-D non-premixed

flame solution with a temperature of 550K for both the fuel and air boundaries. The shear layers in the flame zone develop quickly and velocity fluctuations can be clearly observed within $7\tau_{jet}$.

The DNS was performed for three cases with various Damköhler numbers achieved by different levels of dilution while holding the Reynolds number constant. The case with an intermediate degree of extinction and re-ignition, the $Da = 0.017$ case, is selected for the present study. Fig. 5a shows the mean temperature on the stoichiometric iso-line of the $x - y$ plane centered at $z = 0$, as a function of time. A significant falloff and subsequent recovery of temperature is shown, clearly demonstrating the presence of flame extinction and re-ignition, with local extinction being most significant near $t/\tau_{jet} = 40$ ($t = 0.2\ ms$). Figure 5b shows the standard deviation of temperature on the stoichiometric iso-lines, showing the non-uniformity of flame conditions all over the flow field. Temperature standard deviation significantly increases as the flame becomes partially extinct, and vanishes after the flame re-ignites. Fig. 5c further shows the probability density functions of temperature on the stoichiometric iso-lines for four different time instances. Presence of both low- and high-temperature mixtures on the stoichiometric iso-line can be observed near $t/\tau_{jet} = 40$, indicating a significant extent of flame extinction. The low-temperature mixtures vanish at $t/\tau_{jet} = 80$ ($t = 0.4\ ms$), showing that the flame has largely re-ignited.

4.2 Local extinction and re-ignition

To further show the flame extinction process, 2-D snapshots of the temperature field at the $x - y$ plane centered at $z = 0$ for different time instances are shown in Fig. 6. The top-left

panel shows the initial flame configuration, where two thin flame zones can be observed. At the subsequent time instances, the non-premixed flames are severely disturbed by the strong turbulence. A significant amount of local extinction can be observed at $t/\tau_{jet} = 40$, as indicated by the areas with significantly reduced temperature along the stoichiometric iso-line. Re-ignition is observed at $t/\tau_{jet} = 60$, and strongly burning flame re-established along the stoichiometric iso-line at $t/\tau_{jet} = 80$.

4.3 CEMA-based diagnostics of local extinction and re-ignition

Four snapshots of the CEM eigenvalue are shown in Fig. 7. At $t/\tau_{jet} = 0$, it is seen that the initial flame involves only nonexplosive mixtures in the reaction zone, suggesting that they are strongly burning flames. This is because the flame is initialized by a strongly burning 1-D non-premixed flame, similar to flame P1 in Fig. 4c. At $t/\tau_{jet} = 20$ ($t = 0.1\,ms$), explosive mixtures are observed along the stoichiometric iso-surface, delineating the near- and post-extinction states corresponding to the highly strained flame segments. At $t/\tau_{jet} = 40$, a significant amount of explosive mixtures can be observed along the stoichiometric iso-line, indicating the increased extent of local extinction. At $t/\tau_{jet} = 60$, re-ignition has occurred as mixtures along the bulk section of the stoichiometric iso-surface become nonexplosive. It is seen that the CEMA results are consistent with the temperature information shown in the Fig. 6.

To further show the distribution of the explosive mixtures in the phase space, scatter plots of temperature versus mixture fraction are shown in Fig. 8 for the four time instances. It is seen that the initial temperature profile ($t = 0$) conforms to that of a strongly burning 1-D non-

premixed flame, while significant scatter is present below the strong flame solution, that is the clustered blue dots, can be observed at subsequent time instances. Note that the strongly burning reaction states can be described by near-equilibrium flamelet models, while the explosive mixtures exhibiting a wide degree of scatter may involve fully transient extinction and re-ignition processes, for which the quasi-steady models may not be applicable. It is further observed that the maximum mixture fraction in the fuel core decreases as the flame evolves due to the mixing of O element into the fuel core.

To scrutinize the behaviors of different local flame features in the DNS data, four sub-domains are selected for the 2-D snapshot at $t/\tau_{jet} = 40$ by visually comparing the temperature and eigenvalue plots in Figs. 6 and 7. The three zones marked in Fig. 9a involve distinct local flame features, including strongly burning, near-extinction and post-extinction non-premixed flame segments, respectively. Figures 9b, c and d show the scatter plots of OH mass fraction, a widely adopted flame diagnostic in both experimental and numerical studies, for the three selected sub-domains. The strongly burning flame segment in Fig. 9b resembles flame P1 in Fig. 4 and the initial configuration of the flame in Fig. 6. It is seen that the overall OH concentration is high and the level of scatter is low in the strongly burning flame. The blue dots again indicate the nonexplosive near-equilibrium mixtures. The near-extinction flame segment is shown in Fig. 9c, corresponding to a flame between P2 and P3 in Fig. 4. The near-extinction segment features moderately high temperatures and OH concentrations, while an increased degree of scatter of explosive mixtures is observed in Fig. 9c. Note that the presence of explosive mixtures is a characteristic of the near- and post-extinction flames as discussed above. Figure 9d shows the post-extinction flame segment that is characterized by low temperatures and OH concentrations.

4.4 A premixed flame front in the non-premixed flame

As reviewed in the previous study [15], re-ignition in the flame can possible be attributed to auto-ignition, turbulent folding of the burning regions into extinguished regions, and the propagation of premixed flame fronts. In the present study, the presence of premixed flames in the re-igniting non-premixed flames is further studied using a CEMA based criterion, that is the zero-crossing point of λ_e. Due to the presence of local extinction, which may also induce the eigenvalue zero-crossing, this criterion will be combined with additional physical observations to detect premixed flame fronts in the re-igniting non-premixed flame.

Figure 10 shows the subdomains highlighted in Fig. 9a, which includes a candidate local premixed flame front formed during the re-ignition process. To study the features of the premixed flame segment, Fig. 10a shows the isocontour of progress variable, defined as $c = (T - T_0)/(T_{eq} - T_0)$, where $T_0 = 550K$ is the temperature of fresh mixtures calculated based on non-reactive mixing of fuel and air, and T_{eq} is the adiabatic flame temperature of the local mixture, calculated with the CHEMKIN chemical equilibrium solver at constant-pressure and adiabatic condition. It is seen that the progress variable in the sub-domain increases over a thin layer of O(100) μm, being comparable to a typical reaction zone thickness of a premixed flame, near the isoline for $\lambda_e = 0$, which is possibly a premixed reaction front as discussed in previous studies [17, 18]. It is emphasized again that, due to the presence of local extinction and re-ignition, the eigenvalue zero-crossing alone is not sufficient to distinguish between a premixed reaction front and an extinction front, and thus additional evidence is needed to identify a premixed reaction front.

Figure 10b further shows a scatter plot of the CEM eigenvalue versus the progress variable, superposed with 1-D premixed flame solutions (solid lines). It is seen that the pattern of data scatter in the DNS subdomain resembles that of the 1-D premixed laminar flame solutions both in terms of the zero-crossing locations of the CEM for different equivalence ratios. Hence, these CEM characteristics clearly delineate a propagating premixed front. For comparison, the scatter plot of the CEM eigenvalue versus the progress variable for the near-extinction subdomain marked in Fig. 9 is shown in Fig. 10c, superposed with 1-D solutions for flames P2 and P3 in Fig. 4. A drastically different scattering pattern from that in Fig. 10b is observed. As such, the near-extinction non-premixed flame and premixed fronts can be readily distinguished based on their distinct patterns of scatter shown in Figs. 10b and c.

The propagation of the premixed flame front identified in Fig. 10 is further tracked with a selected subdomain, as indicated by the boxes in Fig. 11. The average x-velocity of the subdomain is approximately 89 m/s, while the maximum y- and z-velocities on the flame front are approximately 7 m/s and 3 m/s, respectively. Therefore the motion perpendicular to the x-y plane is mostly negligible compared with the x-velocity for the subdomain. Note that more accurate tracking of the subdomain can be implemented in 3-D while the visualization can become more involved.

The left column of Fig. 11 shows the temperature field of three consecutive time frames. The black iso-line shows the stoichiometric surface, and the white iso-line indicates $\lambda_e = 0$ which is the premixed reaction front. It is seen that the premixed reaction front propagates from the lower-right corner to the upper-left corner within the three time frames, while the location of the stoichiometric surface remains largely unchanged within the tracked subdomain. The

propagating nature of the premixed reaction front is therefore evident. The right column of Fig. 11 shows the CEM eigenvalue and the progress variable of mixtures in the subdomain. It is seen that the pattern of the CEM eigenvalue scatter resembles that of the 1-D premixed flames in Fig. 10. This result therefore confirms the observation that premixed reaction front can be present in non-premixed flames involving local extinction and re-ignition, and CEMA provides a means to identify the candidate local premixed reaction fronts in such complex flow fields.

5. Conclusions and future work

CEMA is extended to study the behavior of CEM in non-premixed flames involving extinction and re-ignition, based on 1-D steady-state counterflow flames and 3-D DNS data of a temporally evolving turbulent non-premixed ethylene jet flame. For 1-D steady state flames, only nonexplosive mixtures are present when the flame is in strongly burning state, while explosive mixtures emerge near the reaction zone at near- and post-extinction conditions, which provides a necessary condition to detect near- and post-extinction non-premixed flames. The deviation of the λ_e zero-crossing point from the actual extinction point is also observed. Accurate detection of the turning points and further distinction between pre- and post-extinction flames require accurate information on the local mixing timescale, the formulation of which merits further study.

CEMA combined with other scalars, e.g. temperature and species concentrations, can provide quantitative diagnostics to detect complex flame features in turbulent flames. The 3-D DNS of a temporal ethylene jet flame in Ref. [15] is analyzed using CEMA, and the local extinction and re-ignition features in the flame are distinguished and verified. CEMA is also utilized to discover the presence of a premixed reaction front during the re-ignition stage of the non-premixed flame. The premixed reaction front propagates from non-explosive, post-ignition mixtures to explosive, pre-ignition mixtures, which are present in the overall non-premixed flame due to the mixing of fuel and oxidizer after local extinction. The premixed reaction front propagation in a selected subdomain is further verified through comparison with the movement of the stoichiometric surface. The fact that premixed reaction fronts may be present in overall

non-premixed flames involving local extinction and re-ignition leads to the need to consider both premixed and non-premixed flame features in the modeling of such flames.

Future work of this study can include at least two aspects. First, since the present study of the 3-D DNS flame involves only a 2-D slice of the DNS data, investigation using 3-D subdomains may provide more accurate information on flame propagation. Furthermore, it possible to track individual fluid elements, or Lagrangian particles, in the 3-D space to further validate the flame features identified by CEMA. Second, a local mixing timescale τ_s needs to be formulated for general flames, such that the criterion $Da = \lambda_e \cdot \tau_s = 1$ can then be employed to accurately detect the flame extinction states.

References

1. D. o. Energy. *March 2015 Monthly Energy Review*. 2015.

2. M. Stöhr, I. Boxx, C. Carter, and W. Meier, "Dynamics of lean blowout of a swirl-stabilized flame in a gas turbine model combustor," *Proceedings of the Combustion Institute*. 33, 2953-2960 (2011).

3. A. Liñán, "The asymptotic structure of counterflow diffusion flames for large activation energies," *Acta Astronautica*. 1, 1007-1039 (1974).

4. C. K. Law, "Asymptotic theory for ignition and extinction in droplet burning," *Combustion and Flame*. 24, 89-98 (1975).

5. K. Mills and M. Matalon, "Burner-Generated Spherical Diffusion Flames," *Combustion Science and Technology*. 129, 295-319 (1997).

6. F. A. Williams, "Progress in knowledge of flamelet structure and extinction," *Progress in Energy and Combustion Science*. 26, 657-682 (2000).

7. N. Peters, "Laminar diffusion flamelet models in non-premixed turbulent combustion," *Progress in Energy and Combustion Science*. 10, 319-339 (1984).

8. H. Pitsch, C. M. Cha, and S. Fedotov, "Flamelet modelling of non-premixed turbulent combustion with local extinction and re-ignition," *Combustion Theory and Modelling*. 7, 317-332 (2003).

9. J. C. Hewson, "An extinction criterion for nonpremixed flames subject to brief periods of high dissipation rates," *Combustion and Flame*. 160, 887-897 (2013).

10. R. Shan and T. Lu, "Ignition and extinction in perfectly stirred reactors with detailed chemistry," *Combustion and Flame*. 159, 2069-2076 (2012).

11. R. Shan and T. Lu, "A bifurcation analysis for limit flame phenomena of DME/air in perfectly stirred reactors," *Combustion and Flame*. 161, 1716-1723 (2014).

12. P. Sripakagorn, S. Mitarai, Kos, Aacute, G. Ly, and H. Pitsch, "Extinction and reignition in a diffusion flame: a direct numerical simulation study," *Journal of Fluid Mechanics*. 518, 231-259 (2004).

13. R. Venugopal and J. Abraham, "A 2-D DNS investigation of extinction and reignition dynamics in nonpremixed flame–vortex interactions," *Combustion and Flame*. 153, 442-464 (2008).

14. E. R. Hawkes, R. Sankaran, J. C. Sutherland, and J. H. Chen, "Scalar mixing in direct numerical simulations of temporally evolving plane jet flames with skeletal CO/H2 kinetics," *Proceedings of the Combustion Institute*. 31, 1633-1640 (2007).

15. D. O. Lignell, J. H. Chen, and H. A. Schmutz, "Effects of Damköhler number on flame extinction and reignition in turbulent non-premixed flames using DNS," *Combustion and Flame*. 158, 949-963 (2011).

16. C. S. Yoo, E. S. Richardson, R. Sankaran, and J. H. Chen, "A DNS study on the stabilization mechanism of a turbulent lifted ethylene jet flame in highly-heated coflow," *Proceedings of the Combustion Institute*. 33, 1619-1627 (2011).

17. T. F. Lu, C. S. Yoo, J. H. Chen, and C. K. Law, "Three-dimensional direct numerical simulation of a turbulent lifted hydrogen jet flame in heated coflow: a chemical explosive mode analysis," *Journal of Fluid Mechanics*. 652, 45-64 (2010).

18. Z. Luo, C. S. Yoo, E. S. Richardson, J. H. Chen, C. K. Law, and T. Lu, "Chemical explosive mode analysis for a turbulent lifted ethylene jet flame in highly-heated coflow," *Combustion and Flame*. 159, 265-274 (2012).

19. R. Shan, C. S. Yoo, J. H. Chen, and T. Lu, "Computational diagnostics for n-heptane flames with chemical explosive mode analysis," *Combustion and Flame*. 159, 3119-3127 (2012).

20. M. B. Luong, T. Lu, S. H. Chung, and C. S. Yoo, "Direct numerical simulations of the ignition of a lean biodiesel/air mixture with temperature and composition inhomogeneities at high pressure and intermediate temperature," *Combustion and Flame*. 161, 2878-2889 (2014).

21. C. S. Yoo, Z. Luo, T. Lu, H. Kim, and J. H. Chen, "A DNS study of ignition characteristics of a lean iso-octane/air mixture under HCCI and SACI conditions," *Proceedings of the Combustion Institute*. 34, 2985-2993 (2013).

22. M. B. Luong, Z. Luo, T. Lu, S. H. Chung, and C. S. Yoo, "Direct numerical simulations of the ignition of lean primary reference fuel/air mixtures with temperature inhomogeneities," *Combustion and Flame*. 160, 2038-2047 (2013).

23. V. R. Lecoustre, P. G. Arias, S. P. Roy, Z. Luo, D. C. Haworth, H. G. Im, T. F. Lu, and A. Trouvé, "Direct numerical simulations of non-premixed ethylene–air flames: Local flame extinction criterion," *Combustion and Flame*. 161, 2933-2950 (2014).

24. U. Maas and S. B. Pope, "Simplifying chemical kinetics: Intrinsic low-dimensional manifolds in composition space," *Combustion and Flame*. 88, 239-264 (1992).

25. M. Valorani, F. Creta, D. A. Goussis, J. C. Lee, and H. N. Najm, "An automatic procedure for the simplification of chemical kinetic mechanisms based on CSP," *Combustion and Flame*. 146, 29-51 (2006).

26. T. Lu and C. K. Law, "A criterion based on computational singular perturbation for the identification of quasi steady state species: A reduced mechanism for methane oxidation with NO chemistry," *Combustion and Flame*. 154, 761-774 (2008).

27. D. O. Lignell, J. H. Chen, P. J. Smith, T. Lu, and C. K. Law, "The effect of flame structure on soot formation and transport in turbulent nonpremixed flames using direct numerical simulation," *Combustion and Flame*. 151, 2-28 (2007).

28. K. Seshadri and F. A. Williams, "Laminar flow between parallel plates with injection of a reactant at high reynolds number," *International Journal of Heat and Mass Transfer*. 21, 251-253 (1978).

29. M. Kuron, Z. Ren, H. Kolla, E. Hawkes, J. H. Chen, and T. F. Lu. *An Investigation of the Scalar Dissipation Rate Behavior in a Premixed Hydrogen Flame*. in *9th U. S. National Combustion Meeting*, May 17-20, 2015. Cincinnati, Ohio.

Figures

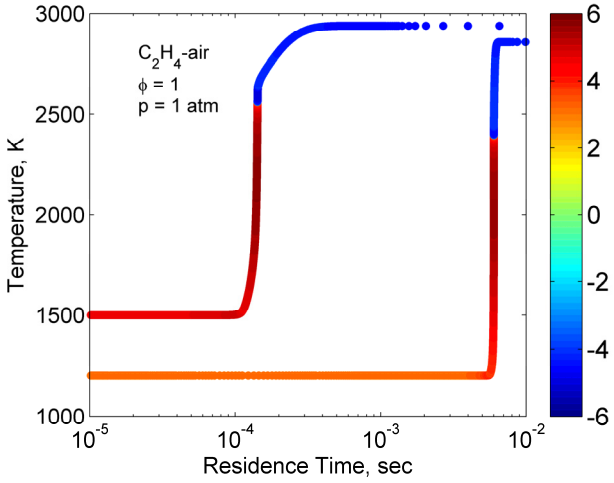

Figure 1. Time dependence of temperature and λ_e in auto-ignition of ethylene-air under constant pressure and initial temperature of 1200 K and 1500 K, respectively. The color of each data point shows the value of $\text{sign}(\lambda_e) \times \log_{10}(|\lambda_e| + 1)$, where "sign" denotes the signum function.

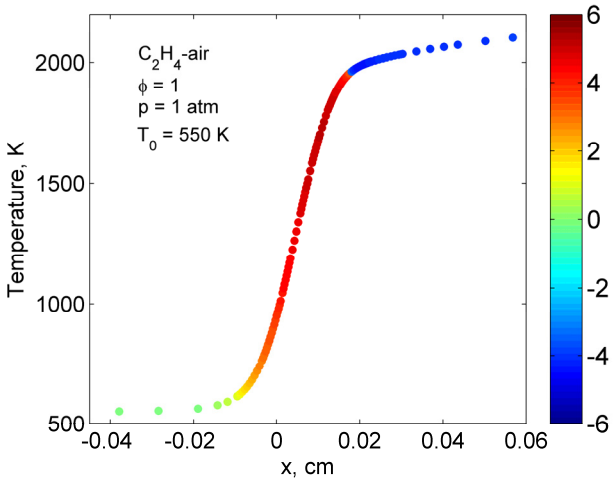

Figure 2. Temperature profile of a 1-D planar freely propagating laminar premixed ethylene-air flame. The color of each data point shows the value of $\mathrm{sign}(\lambda_e) \times \log_{10}(|\lambda_e| + 1)$, where "sign" denotes the signum function.

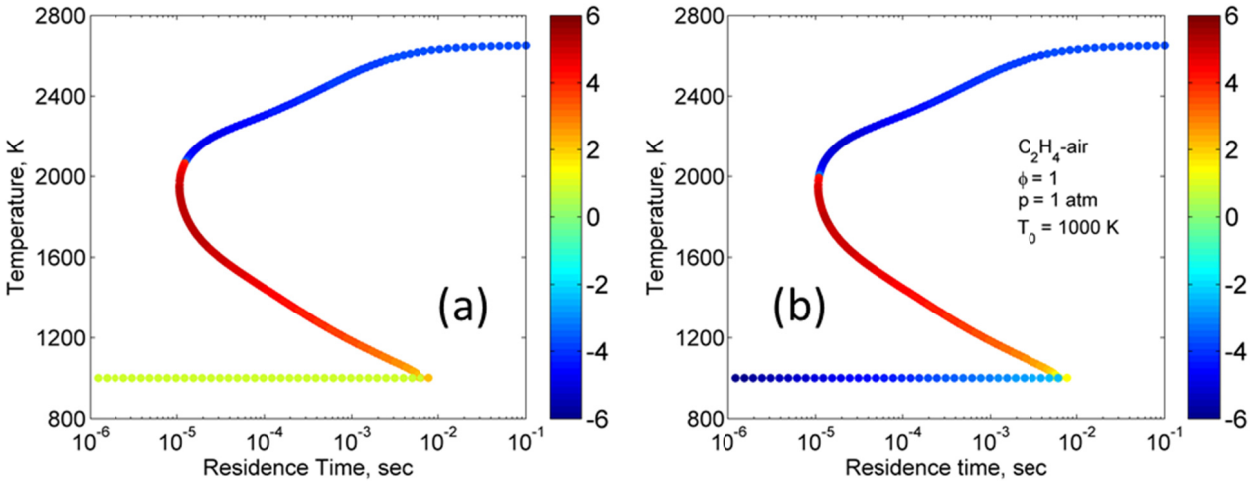

Figure 3. "S"-curve of PSR for stichiometric ethylene-air at atmosperic pressure and inlet tempature of 1000K. The color at each data point shows the value of (a) $\mathrm{sign}(\lambda_e) \times \log_{10}(|\lambda_e| + 1)$ and (b) $\mathrm{sign}(\lambda_e - 1/\tau) \times \log_{10}(|\lambda_e - 1/\tau| + 1)$, where "sign" denotes the signum function and τ is the residence time.

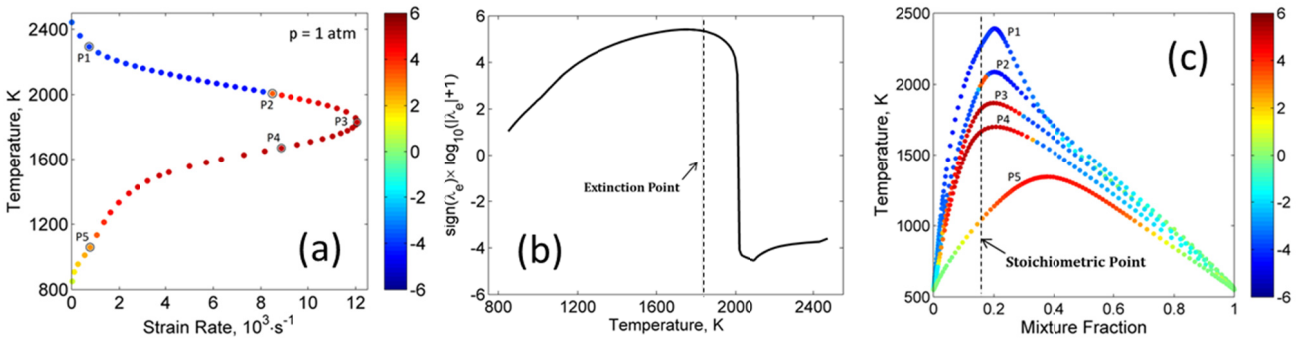

Figure 4. (a) Temperature at the stoichiometric surface as a function of the global strain rate, (b) CEM eigenvalue at the stoichiometric surface as a function of stoichiometric temperature and (c) temperature profiles versus mixture fraction at four selected points on the S-curve, for 1-D steady-state non-premixed counterflow flames of nitrogen diluted ethylene (47.64% ethylene in mole) opposed to nitrogen diluted oxygen (30.53% oxygen in mole) with atmospheric pressure and temperature of 550K at both inlets, calculated with a 19-species reduced mechanism [15, 27]. The color of the data points in (a) and (c) indicates $\text{sign}(\lambda_e) \times \log_{10}(|\lambda_e| + 1)$. The black dashed line in (c) shows the stoichiometric line, where mixture fraction is 0.1587.

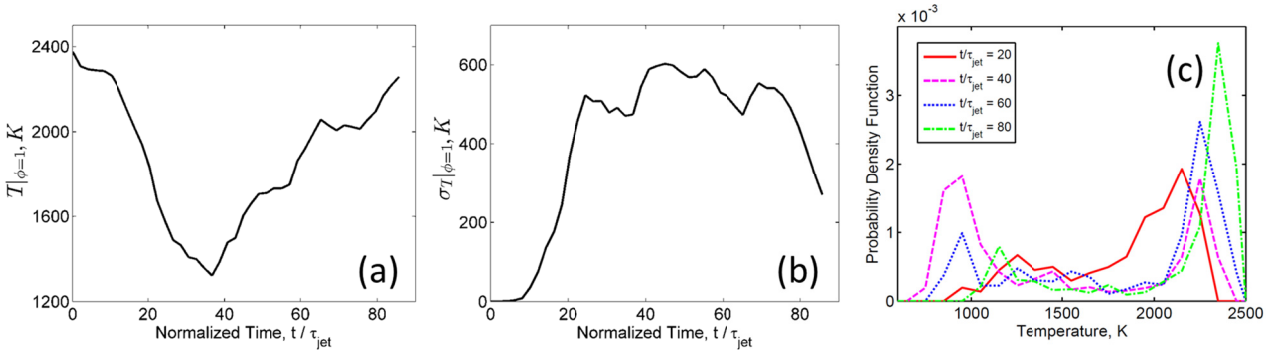

Figure 5. (a) Mean and (b) standard deviation of temperature as functions of time, and (c) probability density functions of temperature for four time instances, on the stoichiometric isoline at the central plane ($z = 0$). Local extinction and re-ignition can be observed through the falloff and recovery of the mean temperature.

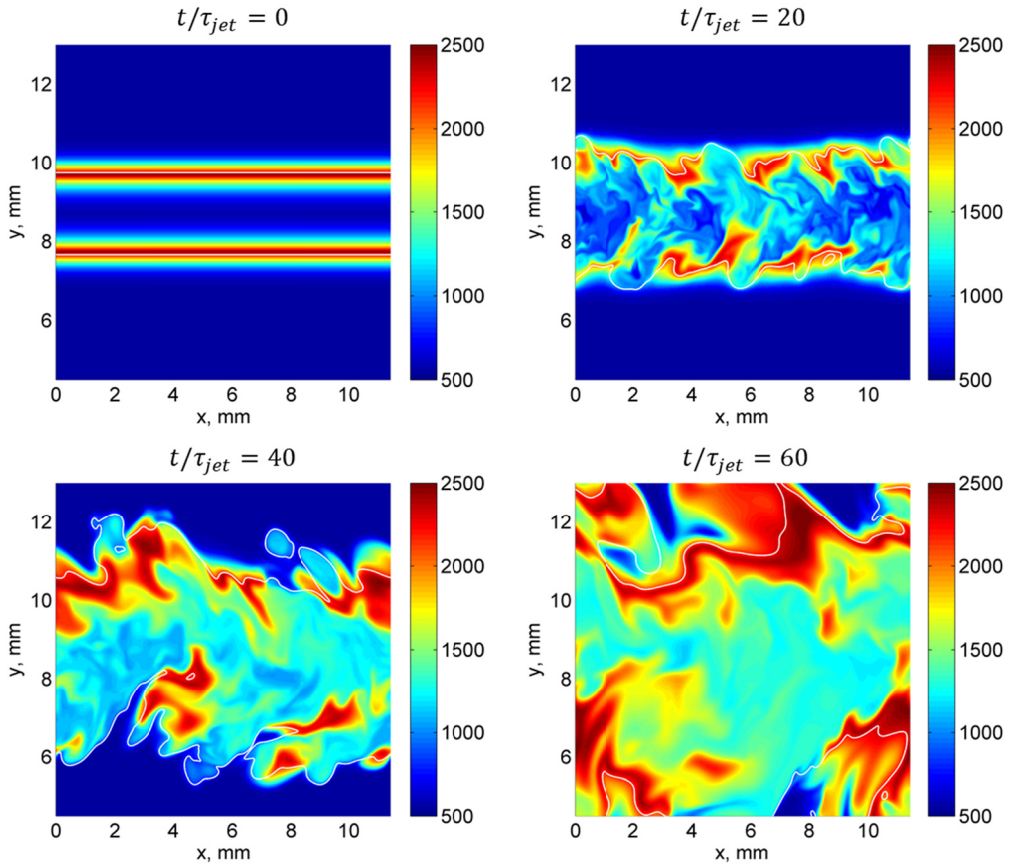

Figure 6. Temperature distribution at the central plane ($z = 0$) of the 3-D non-premixed ethylene jet flame at different time instances, showing the presence of local extinction and re-ignition. White isolines indicate the stoichiometric iso-surface.

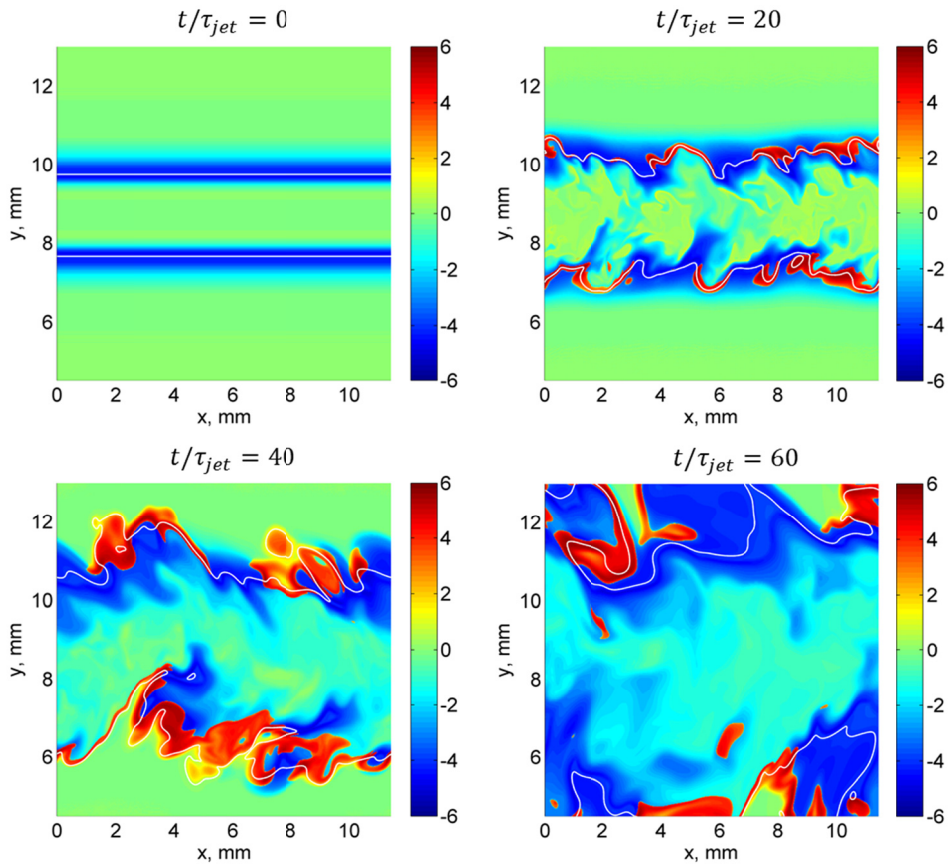

Figure 7. Spatial distribution of λ_e at the central plane ($z = 0$) of the 3-D non-premixed ethylene jet flame at different time instances. White iso-lines indicate the stoichiometric iso-surface.

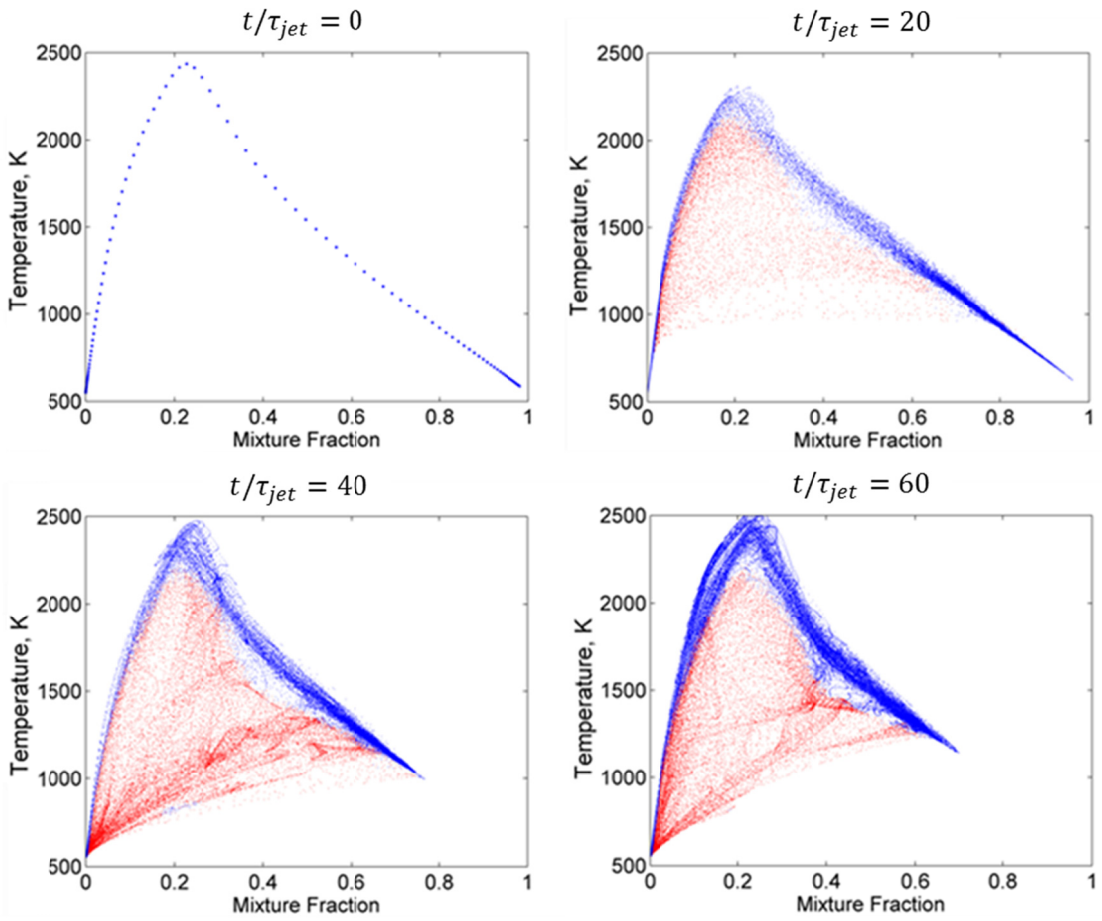

Figure 8. Scatter of temperature versus mixture fraction at different time instances of the non-premixed ethylene jet flame. Blue dots indicate nonexplosive mixtures ($\lambda_e < 0$) and red dots indicate explosive mixtures ($\lambda_e > 0$).

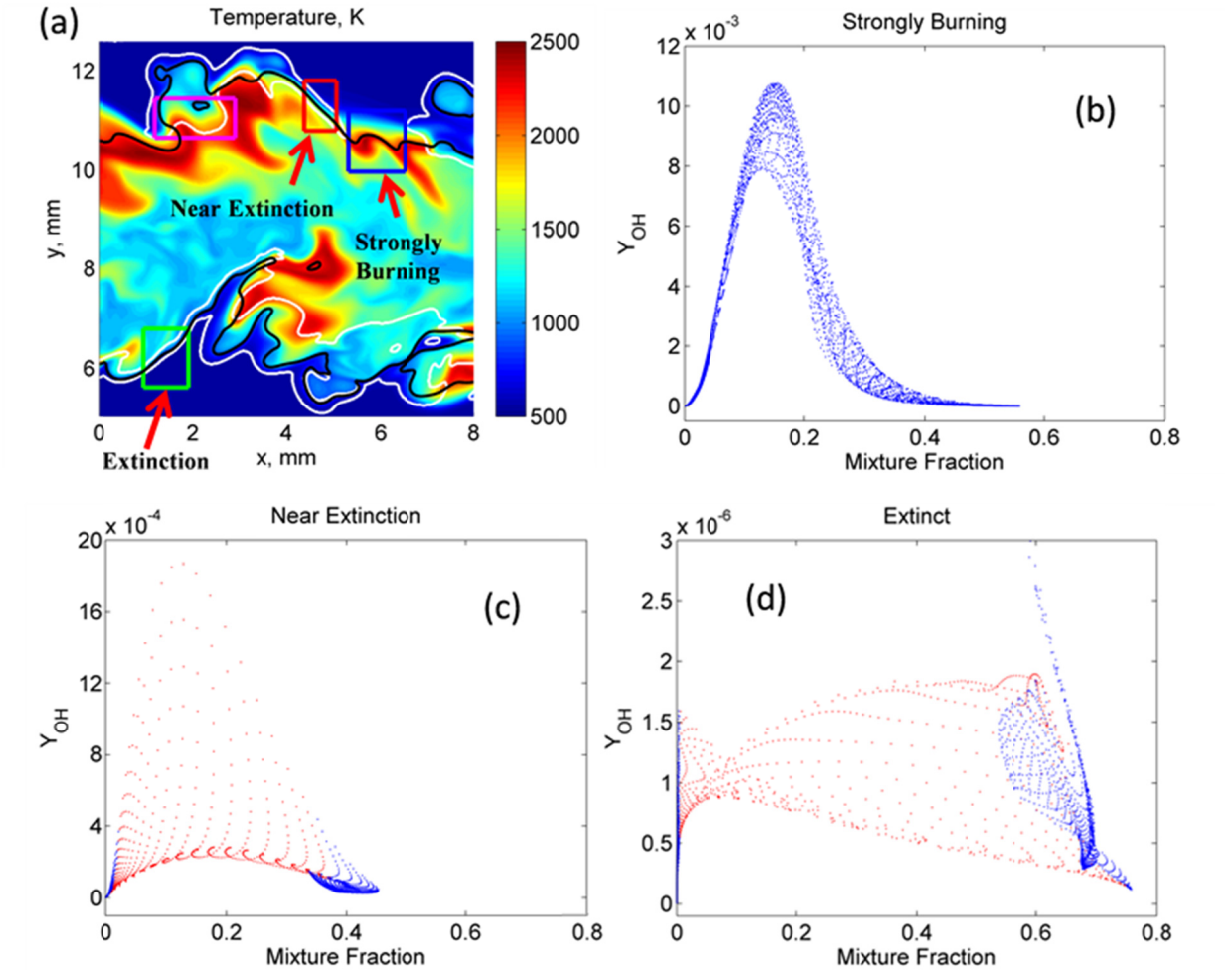

Figure 9. (a) Temperature isocontour at $t/\tau_{jet} = 40$ ($t = 0.2\,ms$), and scatter of OH mass fraction versus mixture fraction in selected flame zones involving (b) strongly burning, (c) near-extinction, and (d) post-extinction non-premixed flame segments. Blue dots in the scatter plots indicate nonexplosive mixtures and red dots indicate explosive mixtures. The white iso-line in (a) indicates $\lambda_e = 0$, and the black isoline indicates the stoichiometric surface.

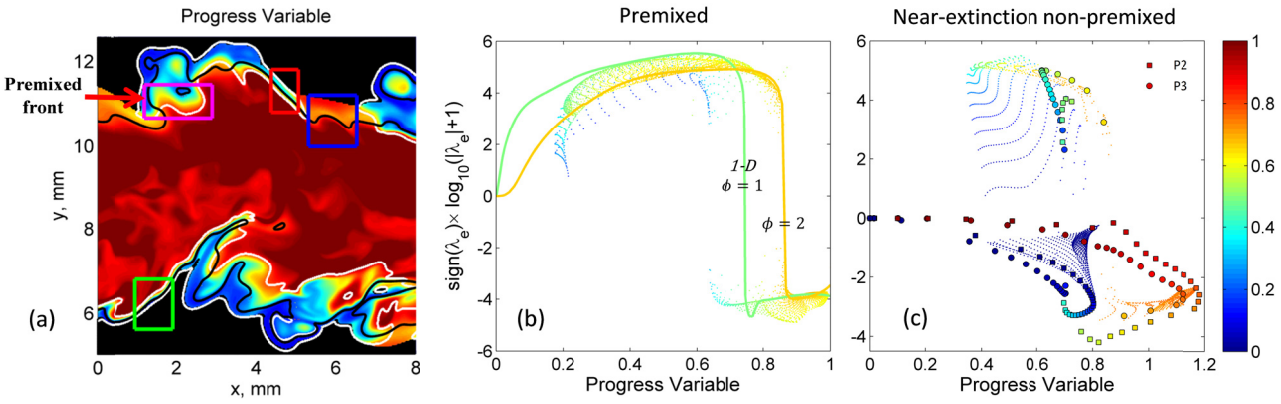

Figure 10. (a) Isocontour of progress variable, (b) scatter of λ_e versus progress variable in the "premixed front" sub-domain (pink box), and (c) scatter of λ_e vs. progress variable in the "near-extinction" sub-domain (red box), of the DNS data at $t/\tau_{jet} = 40$ ($t = 0.2\,ms$). The white isoline in (a) indicates $\lambda_e = 0$, and the black isoline indicates the stoichiometric surface. The solid lines in (b) are unstrained 1-D premixed flame solutions for the mixtures sampled in the DNS at different equivalence ratios, a temperature of $550K$ and atmospheric pressure. The large symbols in (c) indicate 1-D non-premixed flame solutions for flames P2 and P3 in Fig. 4. Colors indicate the progress variable in (a) and the normalized equivalence ratio, $\phi/(\phi + 1)$, in (b) and (c). The area with significantly low equivalence ratio in (a) is truncated to the black color. The larger-than-unity progress variable in (c) indicates the presence of temperature over-shooting.

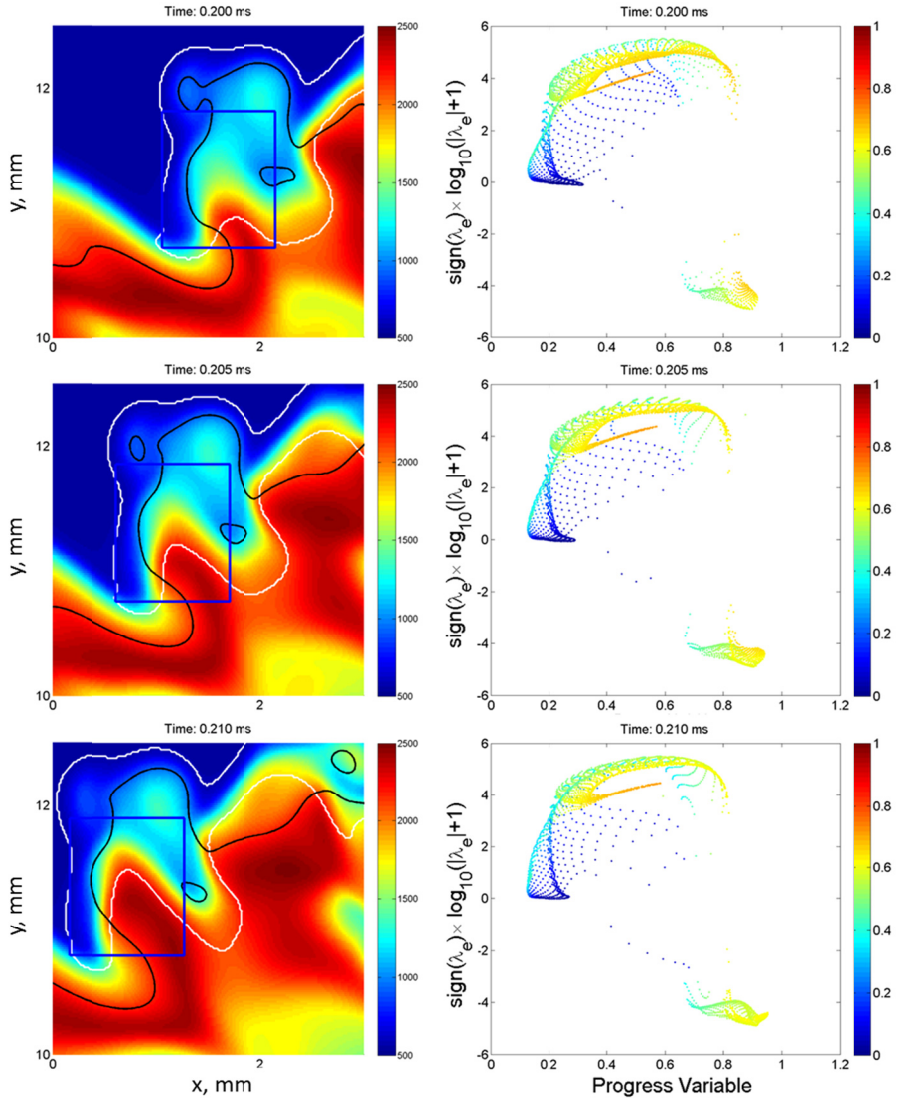

Figure 11. Temperature iscontour (left column) and scatter of λ_e versus the progress variable (right column) in a selected subdomain (the blue box) enclosing a premixed reaction front. The velocity of the subdomain is determined by the mean velocity of the mixtures in the subdomain. The white iso-lines indicate $\lambda_e = 0$, while the black iso-lines are the stoichiometric surface. The color of the symbols in the right column indicates the normalized equivalence ratio, $\phi/(\phi + 1)$.